ORNL
MASTER COPY

**OAK RIDGE NATIONAL LABORATORY**

operated by

UNION CARBIDE CORPORATION

for the

U.S. ATOMIC ENERGY COMMISSION

ORNL-TM-197

# A THERMAL ANALYSIS OF ZIRCALOY FUEL-ELEMENT CONTAINERS FOR THE N. S. SAVANNAH REACTOR

Truman D. Anderson

**NOTICE**

This document contains information of a preliminary nature and was prepared primarily for internal use at the Oak Ridge National Laboratory. It is subject to revision or correction and therefore does not represent a final report. The information is not to be abstracted, reprinted or otherwise given public dissemination without the approval of the ORNL patent branch, Legal and Information Control Department.

LEGAL NOTICE

This report was prepared as an account of Government sponsored work. Neither the United States, nor the Commission, nor any person acting on behalf of the Commission:

A. Makes any warranty or representation, expressed or implied, with respect to the accuracy, completeness, or usefulness of the information contained in this report, or that the use of any information, apparatus, method, or process disclosed in this report may not infringe privately owned rights; or

B. Assumes any liabilities with respect to the use of, or for damages resulting from the use of any information, apparatus, method, or process disclosed in this report.

As used in the above, "person acting on behalf of the Commission" includes any employee or contractor of the Commission, or employee of such contractor, to the extent that such employee or contractor of the Commission, or employee of such contractor prepares, disseminates, or provides access to, any information pursuant to his employment or contract with the Commission, or his employment with such contractor.

ORNL-TM-197

Contract No. W-7405-eng-26

# A THERMAL ANALYSIS OF ZIRCALOY FUEL-ELEMENT CONTAINERS FOR THE N. S. SAVANNAH REACTOR

Truman D. Anderson

Reactor Division

DATE ISSUED

SEP 21 1962

OAK RIDGE NATIONAL LABORATORY
Oak Ridge, Tennessee
operated by
UNION CARBIDE CORPORATION
for the
U.S. ATOMIC ENERGY COMMISSION

## ABSTRACT

Consideration is being given to the substitution of Zircaloy for stainless steel in the fuel-element containers for the N.S. SAVANNAH reactor. A thermal analysis was performed to determine the temperature distributions in the Zircaloy fuel-element container walls and spacer bars; these temperature distributions were obtained primarily for use in evaluating thermal stresses.

The equations for temperature in the fuel-element coolant, control-rod coolant, and container walls were derived; and gamma-ray energy deposition rates in the Zircaloy components were calculated. Three-dimensional temperature distributions in the spacer bars were obtained from numerical solutions of the heat-conduction equation.

Results are presented in the form of temperature-profile curves for each component and for three reactor operating conditions.

# NOMENCLATURE

## Symbols

| | |
|---|---|
| $a$ | thickness of second-pass container wall |
| $b$ | thickness of third-pass container wall |
| $c$ | thickness of follower-rod blade |
| $C_p$ | specific heat of coolant at constant pressure |
| $h$ | coefficient for heat transfer from surface to bulk water |
| $k$ | thermal conductivity |
| $L$ | length of active core |
| $\tilde{L}$ | extrapolated length of reactor core |
| $P$ | core power |
| $P_2$ | second-pass power |
| $P_3$ | third-pass power |
| $Q$ | linear heat rate for one fuel rod |
| $\rho v_4$ | mass coolant flux through control rod slot |
| $S$ | volumetric heat generation rate in solid regions |
| $T$ | temperature |
| $t_4$ | width of control-rod coolant slot |
| $W$ | weight rate of flow through a core coolant pass |
| $w$ | weight rate of flow associated with one fuel rod |

## Subscripts

| | |
|---|---|
| 0 | reactor inlet |
| 2 | second pass |
| 3 | third pass |
| 4 | control-rod slot |
| A | second-pass container wall |
| B | third-pass container wall |
| C | follower rod |

CONTENTS

Page

Abstract ..... iii

Nomenclature ..... v

1. Introduction ..... 1

2. Geometry ..... 5

3. Container-Wall and Coolant Temperature Equations ..... 5

Container Walls ..... 8

Fuel-Element Coolant ..... 9

Control-Rod Coolant ..... 9

4. Heat Transfer Data ..... 11

5. Results for Container Walls and Coolant ..... 12

6. Calculational Method and Results for Spacer Bar ..... 16

APPENDIX A. Derivation of Container-Wall and Coolant Temperature Equations ..... 21

APPENDIX B. Energy Deposition in Zircaloy ..... 29

# A THERMAL ANALYSIS OF ZIRCALOY FUEL-ELEMENT CONTAINERS FOR THE N.S. SAVANNAH REACTOR

## 1. Introduction

Consideration is being given to substituting Zircaloy fuel-element containers for the existing stainless steel containers in the N.S. SAVANNAH reactor. These containers, which form an envelope around each of the 32 fuel elements, are subjected to various stresses arising from pressure differences, fuel-element loading, and temperature variations. The purpose of the analysis presented here was to obtain temperature distributions in the fuel-element containers and associated spacer bars. These temperature distributions were obtained, primarily, for use in evaluating thermal stresses.

A top view of the reactor core assembly is shown in Fig. 1, in which the fuel elements, fuel-element containers, spacer bars (H-shaped pieces separating the containers), and cruciform control rods may be seen. The control rods fit into the spaces between container walls. The fuel-element container assembly without fuel elements and control rods is shown in Fig. 2.

There are three coolant passes within the reactor vessel. The first coolant pass is outside the core. The second-pass coolant flows downward through the outer 16 fuel elements, and the third-pass coolant flows upward through the inner 16 fuel elements. Control-rod coolant flow is also in the upward direction and is in parallel with the third-pass flow. A diagram showing the various reactor coolant flow paths is presented in Fig. 3.

Temperature variations within a given fuel-element container or spacer bar are caused by gamma-ray energy deposition within the part and by variations in coolant temperature around the surface of the part. Temperature variations from part to part are caused by the nonuniform radial power distribution and by the multipass arrangement of the reactor core. Thus, it can be seen that each container or spacer bar has a different temperature than its neighbor. To attempt to describe the temperature of each spacer bar and container in the reactor would not only be a formidable job, but it is very doubtful whether such complete information could be used in a

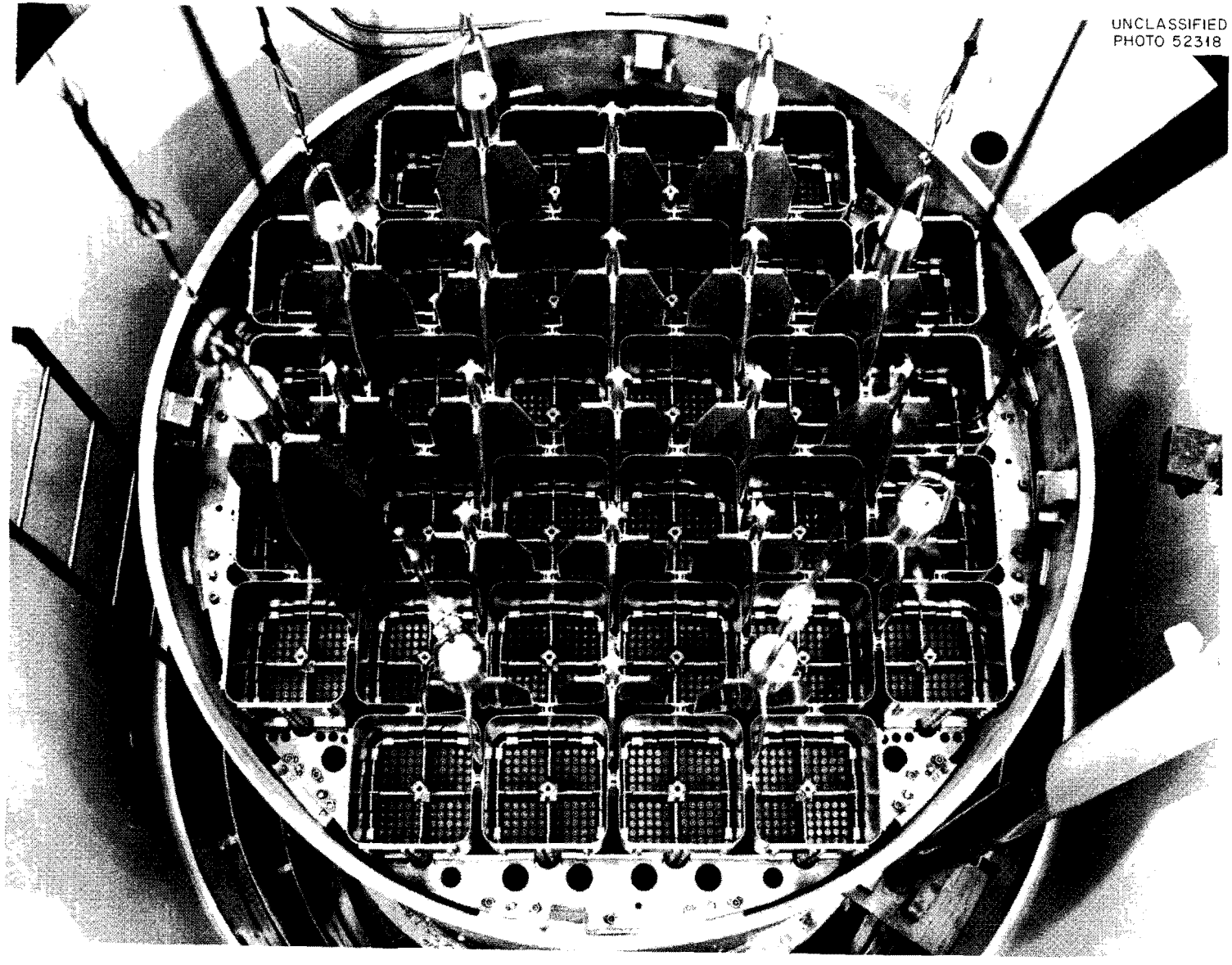


Fig. 1. N.S. SAVANNAH Reactor Core Assembly.

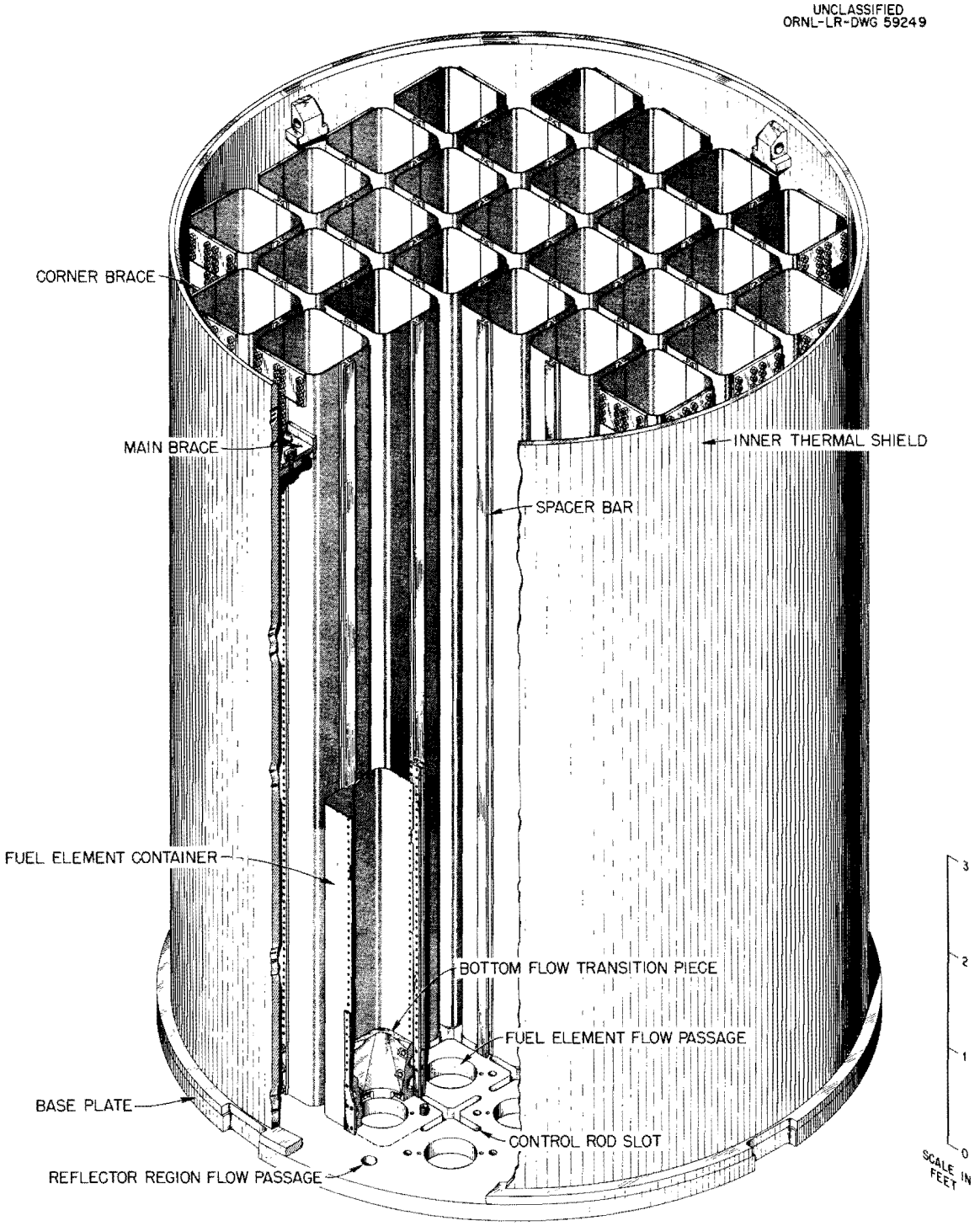


Fig. 2. N.S. SAVANNAH Fuel Element Container Assembly.

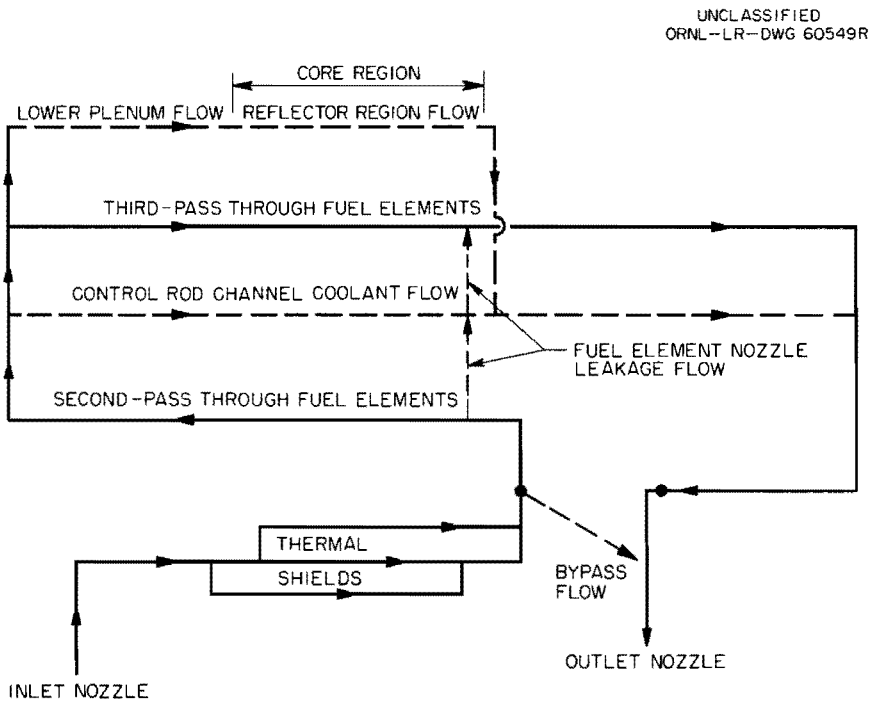


Fig. 3. Diagram of N.S. SAVANNAH Reactor Coolant Flow Paths.

stress analysis. For this reason the thermal analysis was simplified by limiting the analysis to the two adjacent container walls and associated spacer bar that will be subjected to the most severe stress condition.

## 2. Geometry

The largest temperature difference between any two adjacent container walls exists at the boundary between the second and third coolant passes; this comes about because the second-pass coolant has a lower temperature than the third-pass coolant (the container-wall temperatures are, of course, closely coupled to the coolant temperatures). The two fuel elements and associated containers considered in this analysis are the ones shown in Fig. 4, which includes a schematic cross section of the detailed geometry. As may be seen, the follower rod (region C) is touching the third-pass container wall (region B); the interface between the two regions was assumed to be nonconducting. Since there was no physical basis on which to select one follower-rod position over another, the geometry and interface condition that would tend to accentuate the temperature difference between the two container walls was chosen. It may be noted that Fig. 4 is separated into two dash-outlined areas. The lower area was used in obtaining the spacer-bar temperature, and the upper area was of interest in calculating the container-wall temperatures. The arrangement of the upper dash-outlined area suggested a possible simplification to slab geometry. A side view of the slab geometry used in calculating container-wall temperatures is shown in Fig. 5.

## 3. Container-Wall and Coolant Temperature Equations

Since the container walls are thermally coupled to the coolant, it was necessary to develop temperature equations for the second-pass, third-pass, and control-rod coolants, as well as for the container walls. All equations are derived in Appendix A and are presented in the following paragraphs along with the major assumptions and limitations. For orientation relative to coordinates and region designations, reference should be made to Fig. 5.

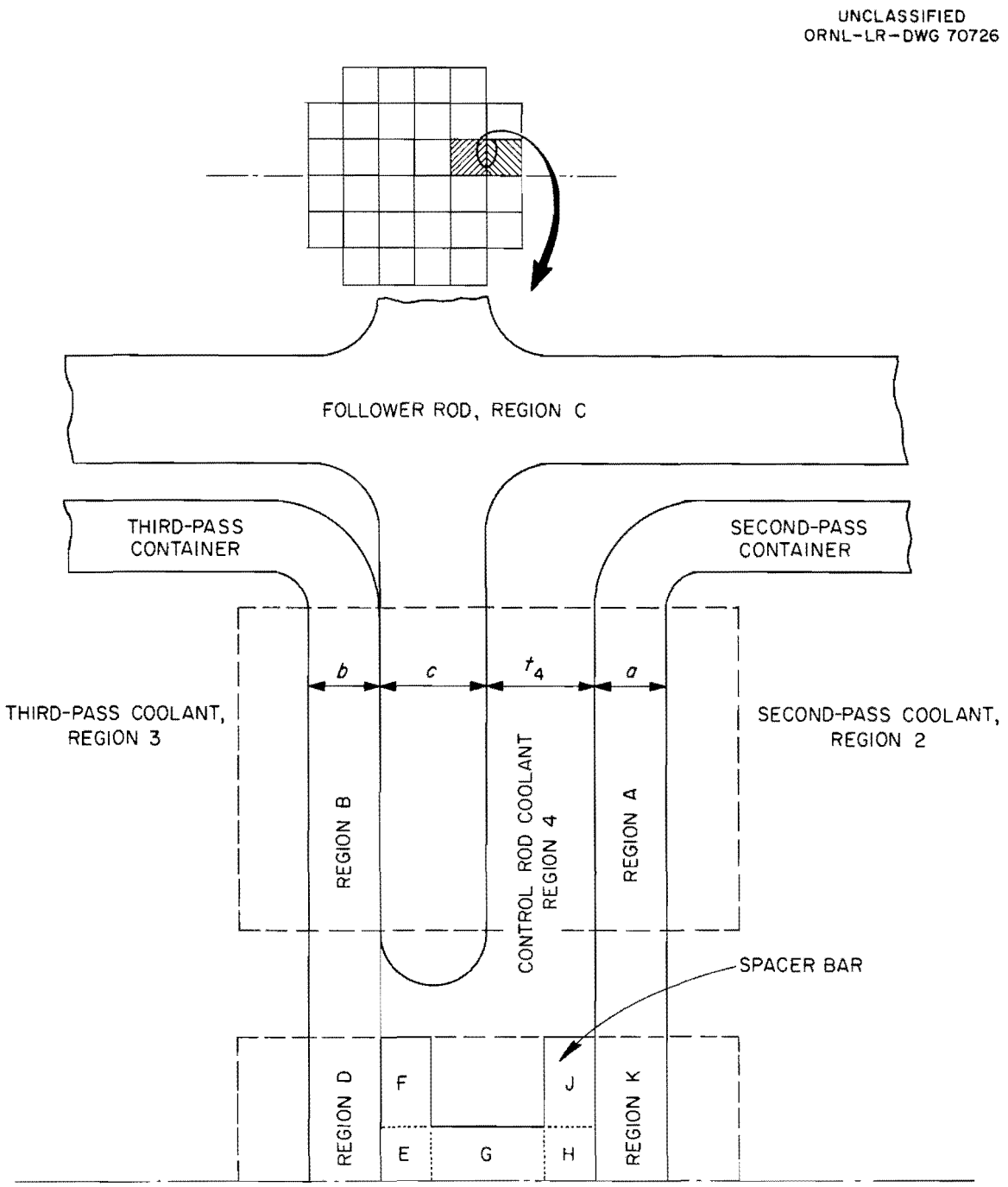


Fig. 4. Core Cross-Section Geometry Used in Thermal Analysis of N.S. SAVANNAH Fuel-Element Containers.

UNCLASSIFIED
ORNL-LR-DWG 70727

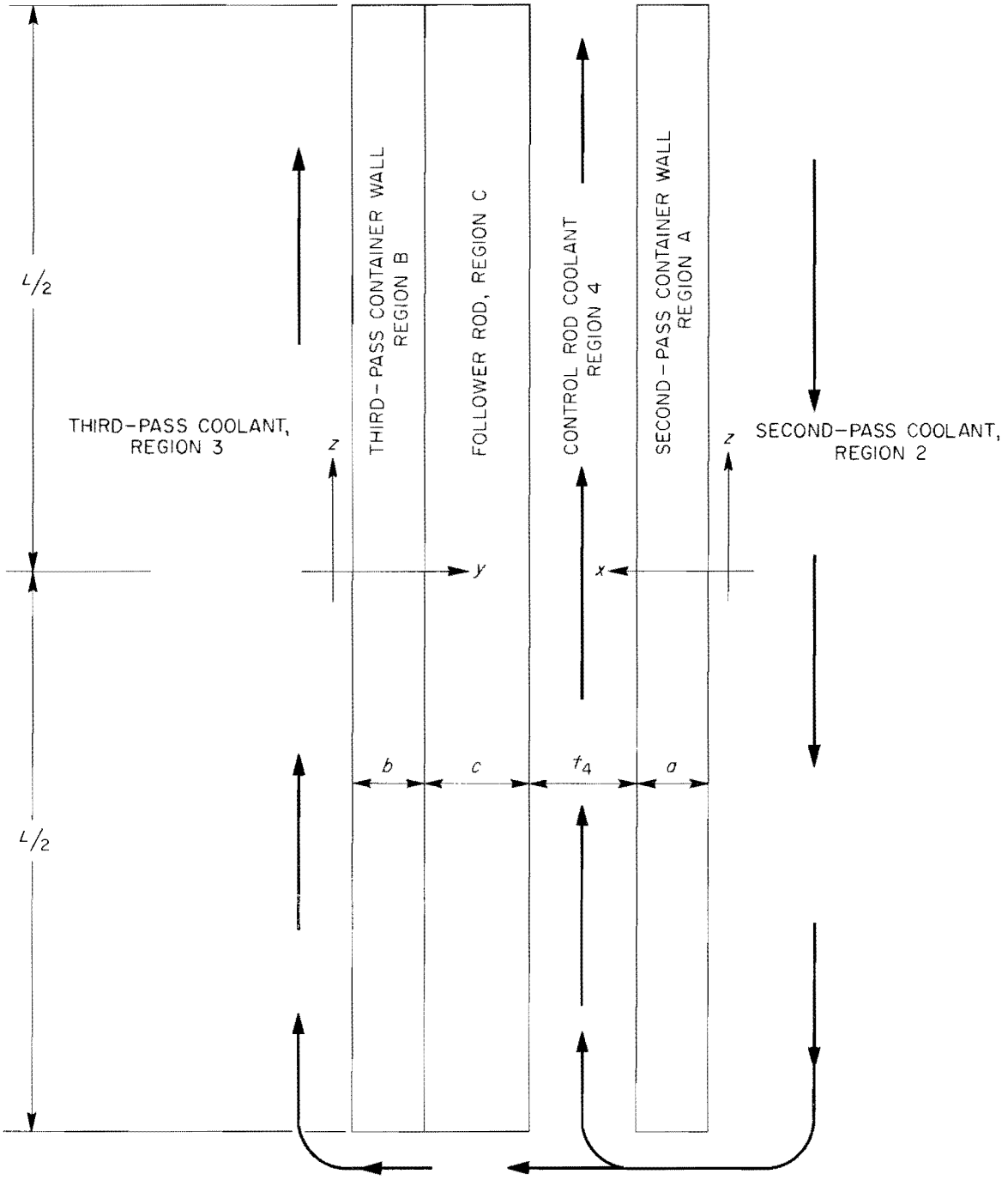


Fig. 5. Slab Geometry Used in Thermal Analysis of Container Walls of N.S. SAVANNAH Fuel Elements.

Container Walls

The main assumptions, other than those concerning geometry, that were used in obtaining the container-wall temperature equations were (1) the previously mentioned insulated interface between regions C and B, (2) zero heat flux in the axial direction (z-direction) for solid regions, and (3) uniform internal heat generation over the thickness of solid regions. The temperature equations for the container walls are

$$T_A(x,z) = T_2(z) - \frac{a^2\, S_A(z)}{2k_A}\left(\frac{x}{a}\right)^2 + \frac{a^2\, S_A(z)}{k_A}\left(\frac{1 + \frac{ah_4}{2k_A}}{1 + \frac{ah_4}{k_A} + \frac{h_4}{h_2}}\right)\left(\frac{x}{a} + \frac{k_A}{ah_2}\right) + \frac{T_4(z) - T_2(z)}{\frac{k_A}{ah_4}\left(1 + \frac{ah_4}{k_A} + \frac{h_4}{h_2}\right)}\left(\frac{x}{a} + \frac{k_A}{ah_2}\right) \tag{1}$$

and

$$T_B(y,z) = T_3(z) - \frac{b^2\, S_B(z)}{2k_B}\left[\left(\frac{y}{b}\right)^2 - 2\left(\frac{y}{b}\right) - \frac{2k_B}{bh_3}\right] . \tag{2}$$

Container-wall temperatures averaged over the wall thickness were obtained from Eqs. (1) and (2) and are

$$\overline{T}_A(z) = T_2(z) - \frac{a^2\, S_A(z)}{6k_A} + \frac{a^2\, S_A(z)}{k_A}\left[\frac{\left(1 + \frac{ah_4}{2k_A}\right)\left(\frac{1}{2} + \frac{k_A}{ah_2}\right)}{1 + \frac{ah_4}{k_A} + \frac{h_4}{h_2}}\right] + \frac{\left[T_4(z) - T_2(z)\right]\left(\frac{1}{2} + \frac{k_A}{ah_2}\right)}{\frac{k_A}{ah_4}\left(1 + \frac{ah_4}{k_A} + \frac{h_4}{h_2}\right)} \tag{3}$$

and

$$\overline{T}_B(z) = T_3(z) + \frac{b^2 \; S_B(z)}{3k_B}\left(1 + \frac{3k_B}{bh_3}\right) \; . \tag{4}$$

Fuel-Element Coolant

As can be seen from Eqs. (1) through (4), calculations of the container-wall temperatures require a knowledge of the fuel-element coolant temperatures $T_2$ and $T_3$. The following major assumptions were made in deriving the fuel-element coolant temperature equations: (1) heat transfer by convection only, (2) temperatures not dependent on heat generated in components other than the fuel element, (3) axial power distribution represented by a chopped cosine, (4) complete coolant mixing between passes, and (5) complete coolant mixing within a fuel element. This latter assumption tends to cause an overestimate of the temperature difference between the adjacent container walls. The resulting temperature equations are

$$T_2(z) = T_0 + \frac{Q_2(0) \; \tilde{L}}{\pi w_2 C_p}\left(\sin \frac{\pi L}{2\tilde{L}} - \sin \frac{\pi z}{\tilde{L}}\right) \tag{5}$$

and

$$T_3(z) = T_0 + \frac{P_2}{W_2 C_p} + \frac{Q_3(0) \; \tilde{L}}{\pi w_3 C_p}\left(\sin \frac{\pi L}{2\tilde{L}} + \sin \frac{\pi z}{\tilde{L}}\right) \; . \tag{6}$$

Control-Rod Coolant

The second-pass container (region A) temperature and the control-rod coolant (region 4) temperature are interdependent. Thus, simultaneous solution of the differential equations describing the temperatures in these two regions was necessary to obtain a coolant-temperature equation not explicitly involving $T_A$. The main assumption was that gamma heating in the solid regions was uniform with respect to all coordinates. This assumption is probably the most restrictive of any made in the analysis.

For small gamma-heating rates, however, the error is small; that is, it is probably not over 2 to 3°F for the control-rod coolant temperatures. The temperature of the control-rod coolant is given by

$$T_4(z) = T_0 + \frac{\tilde{L}\, Q_2(0)}{\pi w_2 C_p} \sin \frac{\pi L}{2\tilde{L}} + \frac{M}{\lambda}$$

$$+ \left[\frac{P_2}{W_2 C_p} - \frac{M}{\lambda} - \frac{\tilde{L}\, Q_2(0)}{\pi w_2 C_p} \sin \frac{\pi L}{2\tilde{L}} \left(1 + \frac{\lambda^2 \tilde{L}^2}{\lambda^2 \tilde{L}^2 + \pi^2}\right)\right.$$

$$\left. - \frac{\lambda \tilde{L}^2\, Q_2(0)}{w_2 C_p(\lambda^2 \tilde{L}^2 + \pi^2)} \cos \frac{\pi L}{2\tilde{L}}\right] e^{-\lambda[z+(L/2)]}$$

$$- \frac{\lambda \tilde{L}^2\, Q_2(0)}{w_2 C_p(\lambda^2 \tilde{L}^2 + \pi^2)} \left(\frac{\lambda \tilde{L}}{\pi} \sin \frac{\pi z}{\tilde{L}} - \cos \frac{\pi z}{\tilde{L}}\right) , \qquad (7)$$

where

$$\lambda = \frac{h_4}{\rho v_4 C_p t_4 \left(1 + \frac{h_4}{h_2} + \frac{a h_4}{k_A}\right)}$$

and

$$M = \frac{1}{\rho v_4 C_p t_4} \left[c S_C + a S_A \left(\frac{\frac{h_4}{h_2} + \frac{a h_4}{2 k_A}}{1 + \frac{h_4}{h_2} + \frac{a h_4}{k_A}}\right)\right].$$

## 4. Heat-Transfer Data

All heat-transfer data used in the calculations are listed in Table 1. Some information about the origin of the more important data is given in the following paragraphs.

Table 1. Values of Constants Used in Thermal Analysis

| | For Operation at 69 Mw with 4 Pumps | For Operation at 89.7 Mw with 4 Pumps | For Operation at 89.7 Mw with 2 Pumps |
|---|---|---|---|
| $S_A = S_B = S_C$, Btu/hr·ft$^3$ | $6.84 \times 10^5$ | $8.89 \times 10^5$ | $8.89 \times 10^5$ |
| $k_A = k_B$, Btu/hr·ft·°F | 7.4 | 7.4 | 7.4 |
| $h_4$, Btu/hr·ft$^2$·°F | 1697 | 1697 | 1173 |
| $h_2$, Btu/hr·ft$^2$·°F | 3670 | 3670 | 2536 |
| $h_3$, Btu/hr·ft$^2$·°F | 3348 | 3348 | 2313 |
| a = b, in.[a] | 0.142 | 0.142 | 0.142 |
| c, in. | 0.375 | 0.375 | 0.375 |
| $t_4$, in. | 0.360 | 0.360 | 0.360 |
| $\tilde{L}$, in.[b] | 69.25 | 69.25 | 69.25 |
| L, in. | 66 | 66 | 66 |
| $W_2$, lb/hr | $7.1 \times 10^6$ | $7.1 \times 10^6$ | $4.47 \times 10^6$ |
| $W_3$, lb/hr | $6.35 \times 10^6$ | $6.35 \times 10^6$ | $4.00 \times 10^6$ |
| $w_2$, lb/hr | $2.706 \times 10^3$ | $2.706 \times 10^3$ | $1.704 \times 10^3$ |
| $w_3$, lb/hr | $2.420 \times 10^3$ | $2.420 \times 10^3$ | $1.524 \times 10^3$ |
| $\rho v_4$, lb/hr·ft$^2$ | $0.726 \times 10^6$ | $0.726 \times 10^6$ | $0.455 \times 10^6$ |
| $C_p$, Btu/lb·°F | 1.186 | 1.186 | 1.186 |
| $P_2$, Btu/hr | $47.9 \times 10^6$ | $97.3 \times 10^6$ | $97.3 \times 10^6$ |
| $Q_2(0)$, Btu/hr·ft | $8.922 \times 10^3$ | $11.6 \times 10^3$ | $11.6 \times 10^3$ |
| $Q_3(0)$, Btu/ft·hr | $16.631 \times 10^3$ | $21.62 \times 10^3$ | $21.62 \times 10^3$ |

[a]In order to perform the thermal analysis, it was necessary to assume a value for the thickness of the container walls. This thickness was chosen as 0.142 in. Since thickness is the quantity to be determined from the stress analysis, however, the assumed value is not necessarily correct.

[b]Chosen to give an axial peak-to-average power of 1.5.

The radial power distribution in the core (with control rods out) was obtained from four-group, two-dimensional, diffusion-theory calculations.[1] The power distribution in the axial direction was a chopped cosine (symmetrical about the core midplane) with a peak-to-average ratio of 1.5.[2]

The coolant flow rates used were obtained from information supplied by The Babcock & Wilcox Company,[3] the reactor designer. Heat transfer coefficients were calculated using the Dittus-Boelter equation.[4] Since there are uncertainties in flow geometries near the container walls because of lateral "play" between the fuel elements and containers, the calculated heat transfer coefficients represent average values.

Calculations of gamma-ray heat-deposition rates in the Zircaloy parts are discussed in Appendix B. It may be noted from Table 1 that the heat deposition rates used in the temperature calculations were uniform throughout the solid regions and were the values appropriate for the core midplane. The use of uniform heat deposition results in overestimates of the temperatures everywhere except at the core midplane.

## 5. Results for Container Walls and Coolant

All coolant and solid-region temperatures were calculated for three reactor operating conditions: (1) operation at 69 Mw with 4 pumps (design condition); (2) operation at 89.7 Mw with four pumps (maximum overpower); and (3) operation at 89.7 Mw with 2 pumps. Coolant temperatures as a function of axial position in the core are given in Figs. 6, 7, and 8. Container-wall temperatures averaged over the thickness are shown in Fig. 9.

---

[1]E. E. Gross, B. W. Colston, and M. L. Winton, Nuclear Analysis of N.S. SAVANNAH Reactor with Zircaloy and Stainless Steel as Fuel-Element Containers, ORNL-3261 (April 24, 1962).

[2]G. E. Kulynych, Nuclear Merchant Ship Reactor Final Safeguards Report — Description of the N.S. SAVANNAH, BAW-1164, Vol. I (June 1960).

[3]Letter, R. F. Ryan (The Babcock & Wilcox Company) to C. R. McFarland, Nuclear Merchant Ship Reactor Core Flow — Pressure Drop Analysis (Dec. 8, 1959).

[4]William H. McAdams, Heat Transmission, 3rd ed., McGraw-Hill, New York, 1954, p. 219.

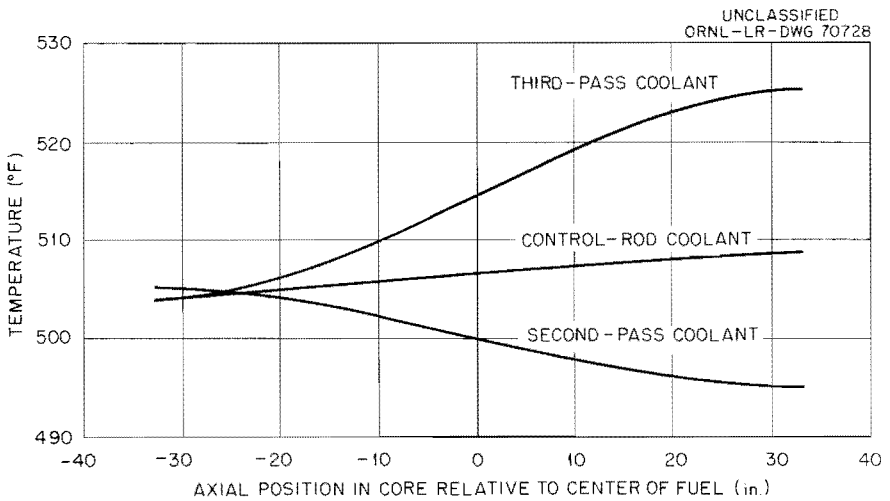


Fig. 6. N.S. SAVANNAH Coolant Temperatures for Four-Pump Operation at 69 Mw.

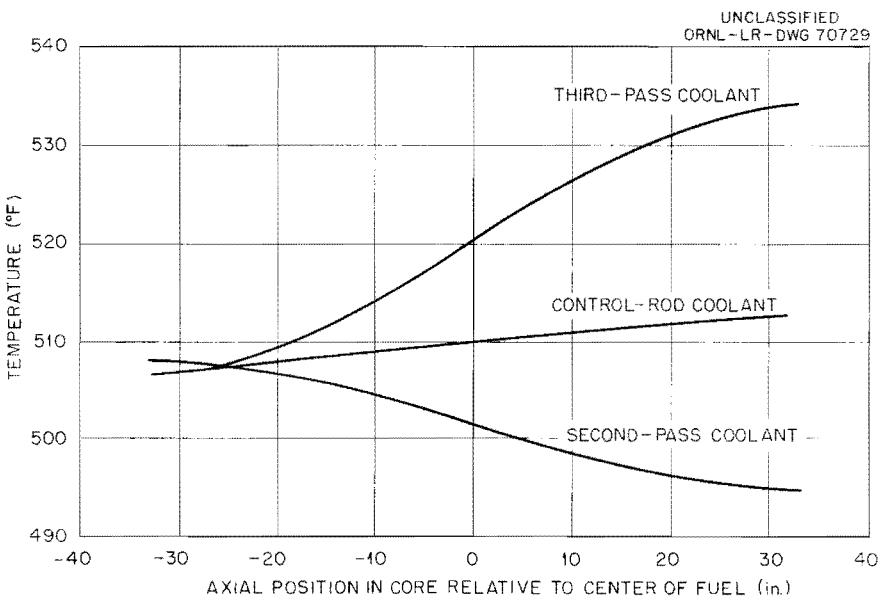


Fig. 7. N.S. SAVANNAH Coolant Temperatures for Four-Pump Operation at 89.7 Mw.

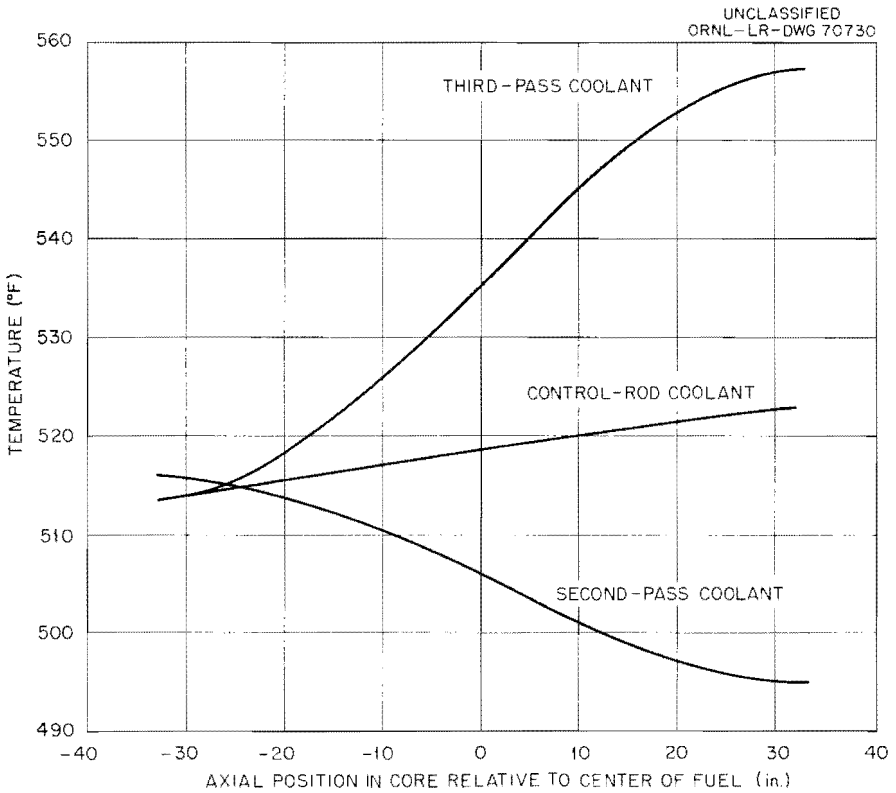


Fig. 8. N.S. SAVANNAH Coolant Temperatures for Two-Pump Operation at 89.7 Mw.

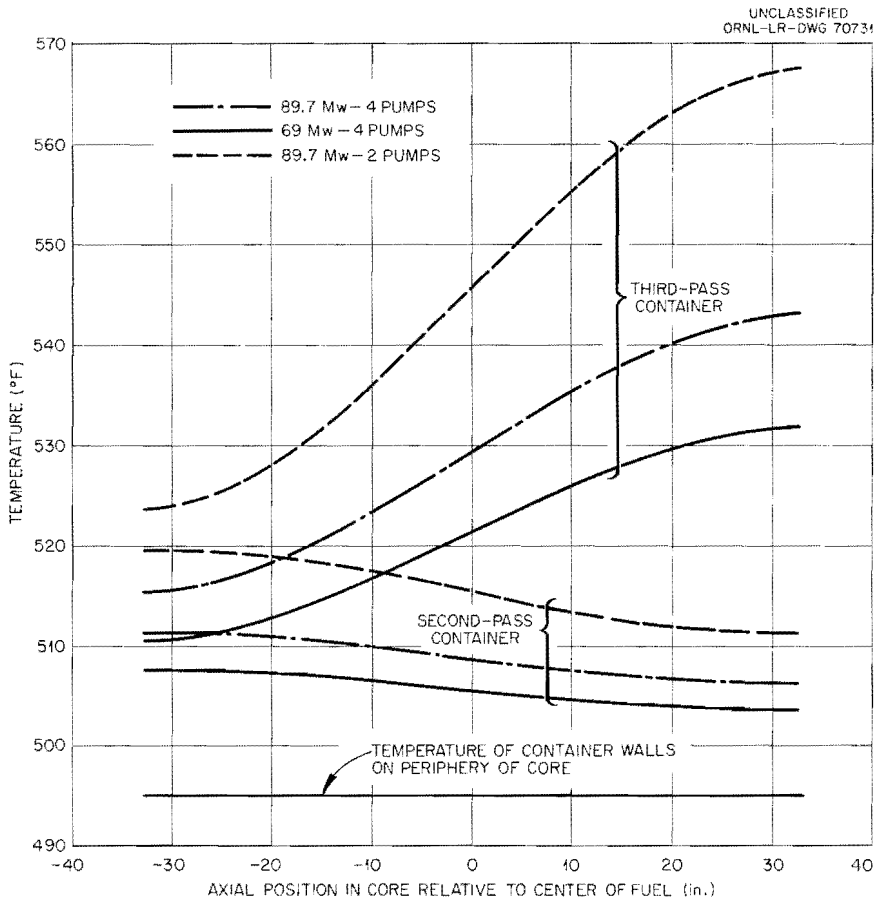


Fig. 9. Average Temperatures in N.S. SAVANNAH Fuel-Element Container Walls.

Temperature profiles across the container walls at the midplane of the core are shown in Fig. 10.

## 6. Calculational Method and Results for Spacer Bar

The spacer-bar temperature distributions were obtained by numerical solutions of the heat-conduction equation using the IBM-7090 digital computer because of the complex geometry and varied boundary conditions. The two-dimensional geometry used in the spacer-bar calculations is shown in the lower dash-outlined area of Fig. 4. In order to use an existing two-dimensional machine code (HOC Code), it was necessary to assume that the heat flux in the axial direction was zero. This assumption is reasonably good for relatively high heat-transfer coefficients, as was the case for this problem. Three-dimensional spacer-bar temperature distributions were obtained by performing the two-dimensional calculations at four axial positions. Convection heat-transfer boundary conditions were used around the surface of the spacer bar. Sink temperatures were obtained from the coolant temperature distributions shown in Figs. 6, 7, and 8.

Axial temperature distributions for the spacer bar are given in Figs. 11, 12, and 13. The temperatures shown are averages for individual regions of the spacer bar. More detailed temperature data are available but were too voluminous for inclusion here.

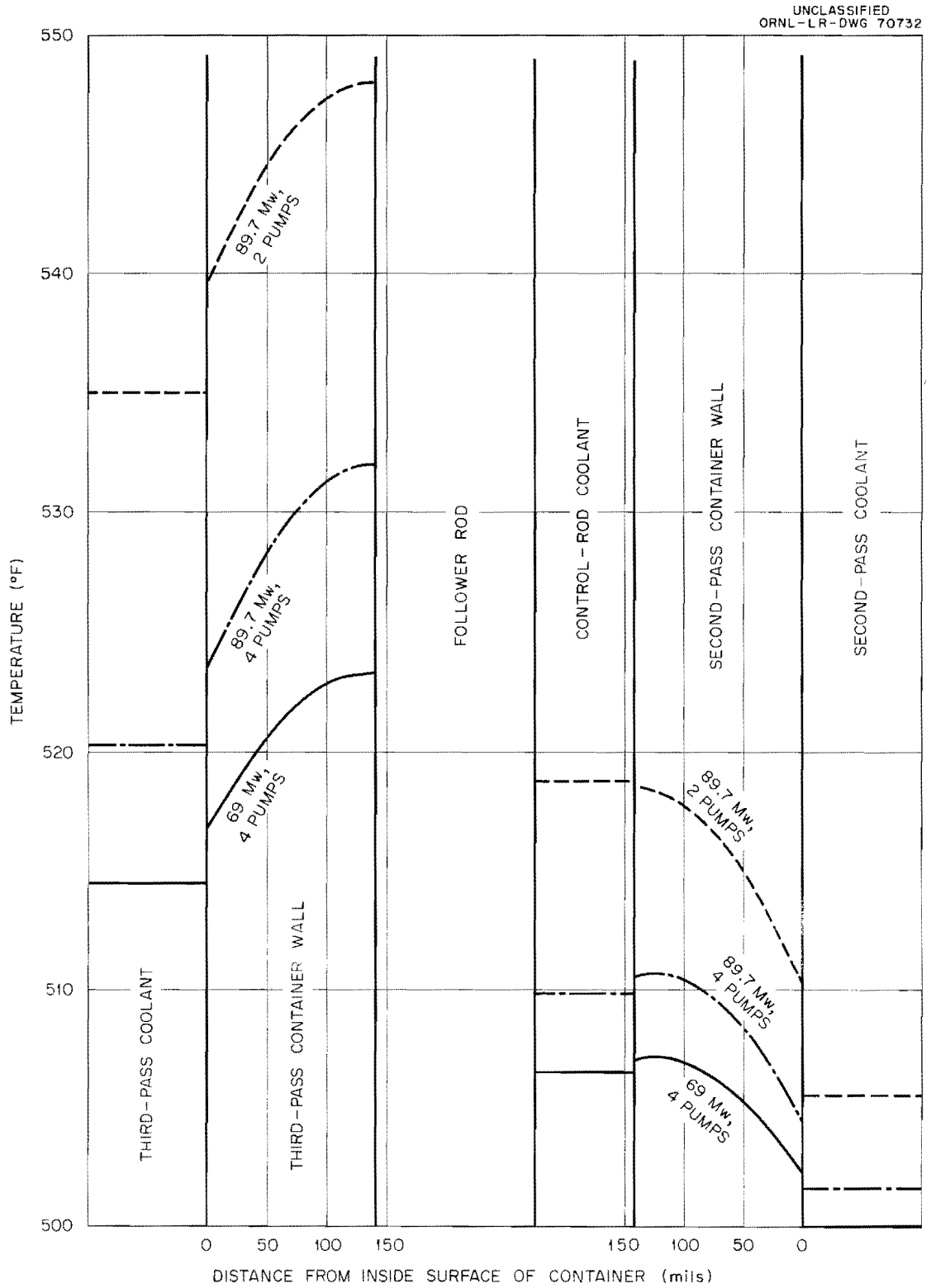


Fig. 10. Temperature Profiles at Midplane of Core of N.S. SAVANNAH.

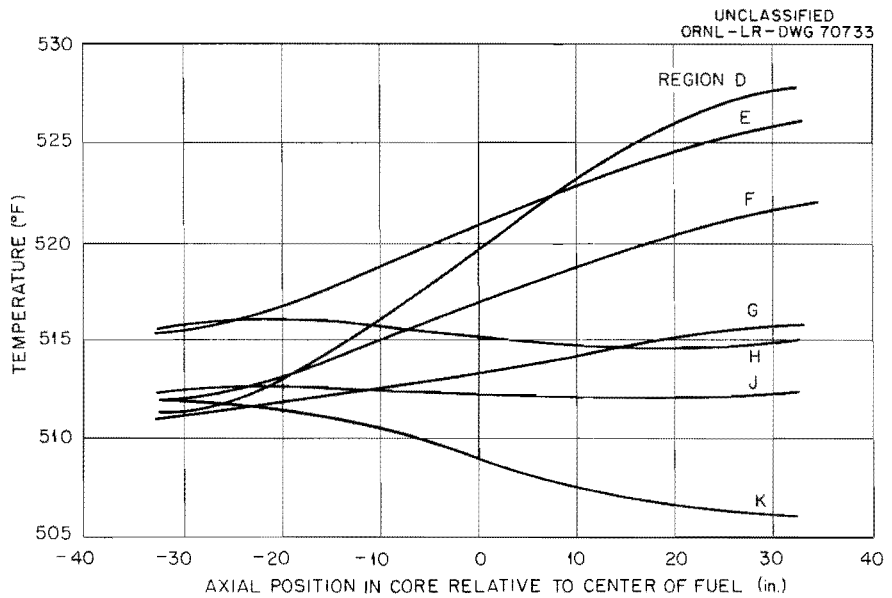


Fig. 11. N.S. SAVANNAH Spacer-Bar Temperature Profiles for Four-Pump Operation at 69 Mw.

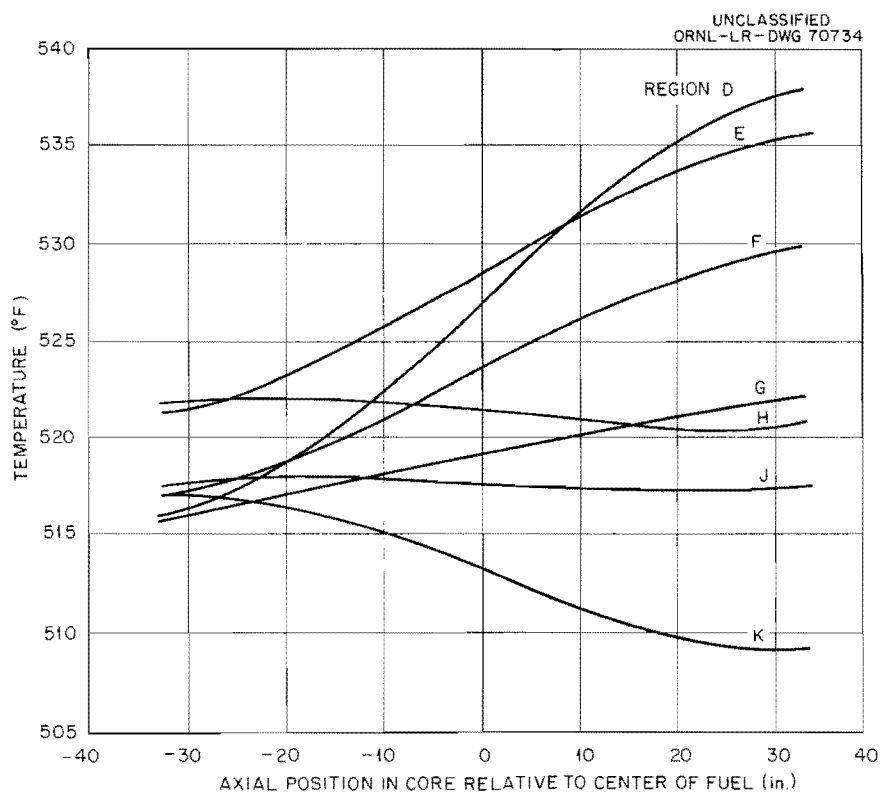


Fig. 12. N.S. SAVANNAH Spacer-Bar Temperature Profiles for Four-Pump Operation at 89.7 Mw.

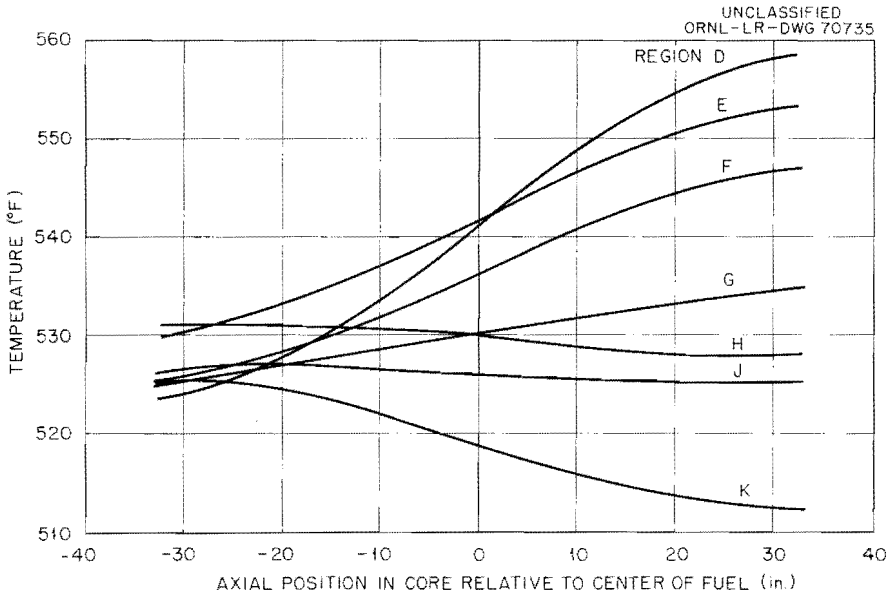


Fig. 13. N.S. SAVANNAH Spacer-Bar Temperature Profiles for Two-Pump Operation at 89.7 Mw.

# APPENDIX A

## DERIVATION OF CONTAINER-WALL AND COOLANT TEMPERATURE EQUATIONS

### Temperature Equations for Container Walls

#### Second-Pass Container Wall (Region A)

There were two major assumptions involved in deriving the equation for temperature in the second-pass container; these assumptions are: (1) there is no conduction in the axial (z) direction and (2) heat generation is uniform with respect to wall thickness. The heat-conduction equation for this case is

$$\nabla^2 T_A(x,z) + \frac{S_A(z)}{k_A} = 0 \quad . \tag{1-A}$$

From the first assumption

$$\frac{\partial^2 T_A(x,z)}{\partial z^2} = 0 \quad ,$$

and Eq. 1-A becomes

$$\frac{\partial^2 T_A(x,z)}{\partial x^2} + \frac{S_A(z)}{k_A} = 0 \quad . \tag{2-A}$$

The convection heat transfer boundary conditions for the problem are

BC 1. $$-k_A \frac{\partial T_A(0,z)}{\partial x} = -h_2 \left[T_A(0,z) - T_2(z)\right] \quad ,$$

BC 2. $$-k_A \frac{\partial T_A(a,z)}{\partial x} = h_4 \left[T_A(a,z) - T_4(z)\right] \quad .$$

Integrating Eq. (2-A) twice gives

$$\frac{\partial T_A(x,z)}{\partial x} = -\frac{S_A(z)\ x}{k_A} + C_1(z) \tag{3-A}$$

and

$$T_A(x,z) = -\frac{S_A(z)\ x^2}{2k_A} + C_1(z)\ x + C_2(z) \quad , \tag{4-A}$$

where $C_1$ and $C_2$ are functions of z only and must be determined from the boundary conditions. From BC 1,

$$C_2(z) = \frac{k_A}{h_2}\ C_1(z) + T_2(z) \quad . \tag{5-A}$$

From BC 2,

$$S_A(z)\ a - k_A\ C_1(z) = h_4 \left[-\frac{S_A(z)\ a^2}{2k_A} + C_1(z)\ a + C_2(z) - T_4(z)\right] \ . \tag{6-A}$$

Combining Eqs. (5-A) and (6-A) and rearranging gives:

$$C_1(z) = \frac{\dfrac{a\ S_A(z)}{k_A}\left(1 + \dfrac{ah_4}{2k_A}\right)}{1 + \dfrac{ah_4}{k_A} + \dfrac{h_4}{h_2}} + \frac{T_4(z) - T_2(z)}{\dfrac{k_A}{h_4}\left(1 + \dfrac{ah_4}{k_A} + \dfrac{h_4}{h_2}\right)} \ . \tag{7-A}$$

Substitution of Eqs. (5-A) and (7-A) into Eq. (4-A) gives the final expression for $T_A$, which is

$$T_A(x,z) = T_2(z) - \frac{a^2\, S_A(z)}{2k_A}\left(\frac{x}{a}\right)^2$$

$$+ \frac{a^2\, S_A(z)}{k_A}\left(\frac{1 + \dfrac{ah_4}{2k_A}}{1 + \dfrac{ah_4}{k_A} + \dfrac{h_4}{h_2}}\right)\left(\frac{x}{a} + \frac{k_A}{ah_2}\right)$$

$$+ \frac{T_4(z) - T_2(z)}{\dfrac{k_A}{ah_4}\left(1 + \dfrac{ah_4}{k_A} + \dfrac{h_4}{h_2}\right)}\left(\frac{x}{a} + \frac{k_A}{ah_2}\right) \quad . \qquad (8\text{-A})$$

Third-Pass Container Wall (Region B)

The basis for obtaining the expression for the third-pass container temperature was the same as for the second-pass container with the exception of boundary conditions. For the third-pass wall, one face was assumed to be insulated. Thus, the boundary conditions are:

BC 1. $$-k_B \frac{\partial T_B(0,z)}{\partial y} = -h_3\left[T_B(0,z) - T_3(z)\right] \quad ,$$

BC 2. $$\frac{\partial T_B(b,z)}{\partial y} = 0 \quad .$$

With these boundary conditions the third-pass container-wall temperature is

$$T_B(y,z) = T_3(z) - \frac{b^2\, S_B(z)}{2k_B}\left[\left(\frac{y}{b}\right)^2 - 2\left(\frac{y}{b}\right) - \frac{2k_B}{bh_3}\right] \quad . \qquad (9\text{-A})$$

## Temperature Equations for Fuel-Element Coolant

A differential equation describing the fuel-element coolant temperature can be obtained by making a heat balance on an incremental volume ($\Delta V$) of a coolant channel; this coolant channel is asssociated with one fuel rod. For a third-pass coolant channel the heat balance is (heat into $\Delta V$ from fuel rod) + (heat into $\Delta V$ by convection) = (heat out of $\Delta V$ by convection) or

$$Q_3(z)\ \Delta z + w_3 C_p\ T_3(z) = w_3 C_p\ T_3(z + \Delta z) \quad . \tag{10-A}$$

Upon dividing through Eq. (10-A) by $\Delta z$, rearranging, and taking the limit as $\Delta z$ tends to zero, it is seen that

$$\frac{dT_3(z)}{dz} = \frac{1}{w_3 C_p}\ Q_3(z) \quad . \tag{11-A}$$

Integration of Eq. (11-A) gives

$$T_3(z) = T_3\left(-\frac{L}{2}\right) + \frac{1}{w_3 C_p} \int_{-L/2}^{z} Q_3(z')\ dz' \quad . \tag{12-A}$$

For an axial power distribution given by

$$Q_3(z) = Q_3(0)\ \cos\frac{\pi z}{\tilde{L}} \quad ,$$

the temperature is

$$T_3(z) = T_3\left(-\frac{L}{2}\right) + \frac{Q_3(0)\ \tilde{L}}{\pi w_3 C_p}\left(\sin\frac{\pi L}{2\tilde{L}} + \sin\frac{\pi z}{\tilde{L}}\right) \quad . \tag{13-A}$$

If complete mixing between the second and third coolant passes is assumed, the third-pass inlet temperature is given by

$$T_3\left(-\frac{L}{2}\right) = T_0 + \frac{P_2}{W_2 C_p} \quad ,$$

and Eq. (13-A) becomes

$$T_3(z) = T_0 + \frac{P_2}{W_2 C_p} + \frac{Q_3(0)\ \tilde{L}}{\pi w_3 C_p}\left(\sin\frac{\pi L}{2\tilde{L}} + \sin\frac{\pi z}{\tilde{L}}\right) \quad . \qquad (14\text{-A})$$

In a manner similar to the above, the second pass coolant temperature can be obtained. The result is

$$T_2(z) = T_0 + \frac{Q_2(0)\ \tilde{L}}{\pi w_2 C_p}\left(\sin\frac{\pi L}{2\tilde{L}} - \sin\frac{\pi z}{\tilde{L}}\right) \quad . \qquad (15\text{-A})$$

## Temperature Equation for Control-Rod Coolant

By making a heat balance on an incremental volume of region 4 of dimensions $\Delta z, t_4, 1$, a differential equation governing the temperature can be obtained. In words, this heat balance is: (heat into $\Delta z, t_4, 1$ by convection) + (heat conducted into $\Delta z, t_4, 1$ from region A) + (heat conducted into $\Delta z, t_4, 1$ from region C) = (heat out of $\Delta z, t_4, 1$ by convection). In terms of the system properties, the heat balance becomes

$$\left[\rho v_4 C_p\ T_4(z)\right]_z t_4 + c\ \Delta z\ S_C(z) + \left[-k_A \frac{\partial T_A(x,z)}{\partial x}\right]_{x=a} \Delta z =$$

$$\left[\rho v_4 C_p\ T_4(z)\right]_{z+\Delta z} t_4 \quad . \qquad (16\text{-A})$$

Rearranging, dividing through by $\Delta z$, and taking the limit as $\Delta z$ tends to zero, it is seen that

$$\frac{dT_4(z)}{dz} = \frac{c\ S_C(z)}{\rho v_4 C_p t_4} - \frac{k_A}{\rho v_4 C_p t_4}\left[\frac{\partial T_A(a,z)}{\partial x}\right] . \tag{17-A}$$

From Eqs. (3-A) and (7-A)

$$k_A \frac{\partial T_A(a,z)}{\partial x} = -S_A(z)\ a + \frac{S_A(z)\ a\left(1 + \frac{ah_4}{2k_A}\right)}{1 + \frac{ah_4}{k_A} + \frac{h_4}{h_2}} + \frac{h_4\ (T_4 - T_2)}{1 + \frac{ah_4}{k_A} + \frac{h_4}{h_2}} . \tag{18-A}$$

Substitution of Eq. (18-A) into Eq. (17-A) gives

$$\frac{dT_4(z)}{dz} + \lambda\ T_4(z) = M(z) + \lambda\ T_2(z) \quad , \tag{19-A}$$

where

$$\lambda = \frac{h_4}{\rho v_4 C_p t_4 \left(1 + \frac{h_4}{h_2} + \frac{ah_4}{k_A}\right)} ,$$

$$M(z) = \frac{1}{\rho v_4 C_p t_4}\left[c\ S_C(z) + a\ S_A(z)\left(\frac{\frac{h_4}{h_2} + \frac{ah_4}{2k_A}}{1 + \frac{h_4}{h_2} + \frac{ah_4}{k_A}}\right)\right] .$$

Using the integrating factor, $e^{\lambda z}$, Eq. (19-A) becomes

$$\frac{d}{dz}\left[e^{\lambda z}\ T_4(z)\right] = e^{\lambda z}\left[M(z) + \lambda\ T_2(z)\right] . \tag{20-A}$$

Integration of Eq. (20-A) gives

$$e^{\lambda z}\, T_4(z) - e^{-\lambda L/2}\, T_4\left(-\frac{L}{2}\right) = \int_{-L/2}^{z} e^{\lambda z'}\, [M(z') + \lambda\, T_2(z')]\, dz'$$

or

$$T_4(z) = e^{-\lambda[z+(L/2)]}\, T_4\left(-\frac{L}{2}\right) + e^{-\lambda z} \int_{-L/2}^{z} e^{\lambda z'} \left[M(z') + \lambda\, T_2(z')\right] dz' \quad . \qquad (21\text{-A})$$

For the case in which $T_2(z)$ is given by Eq. (15-A) and $M(z)$ is uniform with respect to z (i.e., heat generation in solid regions not a function of axial position), the control-rod coolant temperature is

$$\begin{aligned} T_4(z) = T_0 &+ \frac{\tilde{L}\, Q_2(0)}{\pi w_2 C_p} \sin\frac{\pi L}{2\tilde{L}} + \frac{M}{\lambda} \\ &+ \left[\frac{P_2}{W_2 C_p} - \frac{M}{\lambda} - \frac{\tilde{L}\, Q_2(0)}{\pi w_2 C_p} \sin\frac{\pi L}{2\tilde{L}} \left(1 + \frac{\lambda^2 \tilde{L}^2}{\lambda^2 \tilde{L}^2 + \pi^2}\right)\right. \\ &\left. - \frac{\lambda \tilde{L}^2\, Q_2(0)}{w_2 C_p (\lambda^2 \tilde{L}^2 + \pi^2)} \cos\frac{\pi L}{2\tilde{L}}\right] e^{-\lambda[z+(L/2)]} \\ &- \frac{\lambda \tilde{L}^2\, Q_2(0)}{w_2 C_p (\lambda^2\, \tilde{L}^2 + \pi^2)} \left(\frac{\lambda \tilde{L}}{\pi} \sin\frac{\pi z}{\tilde{L}} - \cos\frac{\pi z}{\tilde{L}}\right) \quad . \qquad (22\text{-A}) \end{aligned}$$

# APPENDIX B

## ENERGY DEPOSITION IN ZIRCALOY

### Geometry

The geometry chosen for the gamma-heating calculations, as shown in Fig. B.1, consists of a half-space of homogenized core containing a thin slab of Zircaloy which represents the fuel-element container walls. The Zircaloy slab is positioned a distance "t" (the width of a fuel element) from the face.

### Equations of Gamma-Ray Energy Deposition from Volume Distributed Source

The heat deposition rate at point "P" (see Fig. B.1) from a monoenergetic point source of gamma rays located a distance R away is

$$D_{pt}(R) = S_{pt}\ G(R) \quad , \tag{1-B}$$

where

$S_{pt}$ = energy emission rate of point source,

$G(R)$ = energy absorption rate density at point "P" from a source of unit strength located a distance R away.

The point kernel, $G(R)$, is given by

$$G(R) = \frac{\mu_a B_a\ e^{-\mu R}}{4\pi R^2} \quad , \tag{2-B}$$

where

$\mu$ = total linear attenuation coefficient for the attenuating medium, a function of gamma-ray energy,

$B_a$ = energy-absorption buildup factor for a point isotropic source in the attenuating medium, a function of $\mu R$ and gamma-ray energy,

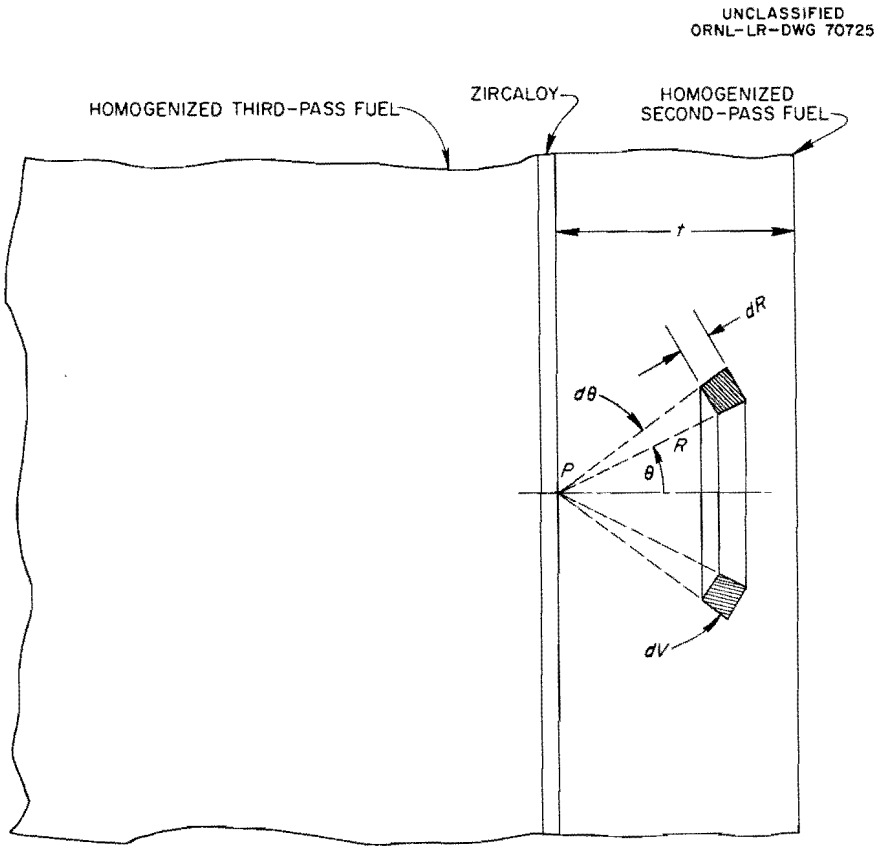


Fig. B.1. Geometry Used in Gamma-Ray Energy Deposition Calculations for Zircaloy Fuel-Element Containers for N.S. SAVANNAH Reactor.

$\mu_a$ = energy-absorption linear attenuation coefficient for the material at the deposition point.*

For a volume-distributed source

$$S_{pt} = S_v \, dV \quad ,$$

where

$S_v$ = energy emission rate per unit volume,

$dV$ = increment of volume.

The energy absorption rate density at point "P" from the total volume, V, is

$$D(P) = \int_V \frac{S_v \mu_a B_a \, e^{-\mu R}}{4\pi R^2} \, dV \quad . \tag{3-B}$$

Using the double exponential form of the buildup factor suggested by Taylor,[1]

$$B_a = A \, e^{-\alpha_1 \mu R} + (1 - A) \, e^{-\alpha_2 \mu R} \quad . \tag{4-B}$$

For the geometry shown in Fig. B.1,

$$dV = 2\pi R^2 \, dR \sin \theta \, d\theta \quad . \tag{5-B}$$

---

*By the definition of the buildup factor, Eq. 2-B is strictly valid only for calculating energy deposition in the attenuating medium. However, if the energy dependence of the energy absorption coefficient in the attenuating material is similar to that in the material in which energy deposition is to be calculated, then it is valid to use $\mu_a$ for the latter material; in this case, Eq. 2-B is useful for calculating energy deposition in materials other than the attenuating medium. The energy dependence of the energy absorption coefficient for the homogenized core material is very similar to that for Zircaloy except at low energies. The buildup of low energy photons in the core mixture, however, is expected to be small due to photoelectric absorptions in uranium. Thus, the use of Eq. 2-B for calculating energy absorption in Zircaloy would appear to be reasonably valid.

[1]J. J. Taylor, Application of Gamma-Ray Buildup Data to Shield Design, WAPD-Memo RM-217 (Jan. 25, 1954).

Combining Eqs. (3-B), (4-B), and (5-B), the energy deposition from a slab of thickness "t" is given by

$$D(P) = \frac{S_v A \mu_a}{2} \int_{\theta=0}^{\pi/2} \int_{R=0}^{t \sec \theta} e^{-(1+\alpha_1)\mu R} \, dR \sin \theta \, d\theta$$

$$+ \frac{S_v (1 - A) \mu_a}{2} \int_{\theta=0}^{\pi/2} \int_{R=0}^{t \sec \theta} e^{-(1+\alpha_2)\mu R} \, dR \sin \theta \, d\theta \quad . \qquad (6\text{-B})$$

Using the relationship

$$\sin \theta \, d\theta = \frac{d(\sec \theta)}{\sec^2 \theta} \quad ,$$

Eq. (6-B) can be integrated to give

$$D(P) = \frac{S_v \mu_a}{2\mu} \left\{ \frac{A}{(1 + \alpha_1)} \left[1 - E_2(\mu_1 t)\right] + \frac{(1 - A)}{(1 + \alpha_2)} \left[1 - E_2(\mu_2 t)\right] \right\} \quad , \qquad (7\text{-B})$$

where

$$E_2(\mu t) = \mu t \int_{\mu t}^{\infty} \frac{e^{-x}}{x^2} \, dx,$$

$$\mu_1 = (1 + \alpha_1) \, \mu,$$

$$\mu_2 = (1 + \alpha_2) \, \mu.$$

The $E_2$ function is tabulated numerous places; for example see ref. 2. For a thick slab, Eq. (7-B) becomes

$$D(P) = \frac{S_v \mu_a}{2\mu} \left[ \frac{A}{(1 + \alpha_1)} + \frac{(1 - A)}{(1 + \alpha_2)} \right] \quad . \qquad (8\text{-B})$$

---

[2]Herbert Goldstein, Fundamental Aspects of Reactor Shielding, Addison-Wesley Publishing Company, Inc., Reading, Massachusetts, 1959.

Equation (7-B) was used to calculate heating in the Zircaloy from gammas originating in the second-pass fuel (see Fig. B.1); and Eq. (8-B) was used for gammas originating in the third-pass fuel.

## Gamma-Ray Source Strength

In calculating source strength, gamma-rays originating from $(n,\gamma)$ reactions in fuel-element materials, fission, and fission-product decay were considered.

The average fission rate density for the core per megawatt of power is $1.164 \times 10^{10}$ fissions/sec·cm$^3$; this figure is based on energy deposition in the core of 200 Mev per fission and a core volume corresponding to that enclosed by the fuel-element containers. The core power density of interest in this calculation was that of the outer third-pass fuel element that is adjacent to the core cross-section centerline. The average fission rate density in this element relative to the core average is 1.346; this figure was obtained from four-group, two-dimensional, diffusion-theory calculations.[3] The axial peak-to-average power was taken to be 1.5.[4]

The number of $(n,\gamma)$ reactions in the fuel-element materials per fission was obtained from four-group, $S_n$, transport-theory calculations,[3] and the results are included in Table B.1. Also shown in Table B.1 are the $(n,\gamma)$ reaction rate densities for various fuel-element materials.

The gamma-ray energy spectrum was approximated by seven discreet energy groups. Capture gamma-ray spectra for the fuel element materials are given in Table B.2. Table B.3 shows the spectra for gammas resulting from fission-product decay. Gamma-ray source strengths by energy groups and by origin are shown in Table B.4.

---

[3]E. E. Gross, B. W. Colston, and M. L. Winton, Nuclear Analysis of N.S. SAVANNAH Reactor with Zircaloy and Stainless Steel as Fuel Element-Containers, ORNL-3261 (April 24, 1962).

[4]G. E. Kulynych, Nuclear Merchant Ship Reactor Final Safeguards Report — Description of the N.S. SAVANNAH, BAW-1164, Vol. I (June 1960).

Table B.1. The (n,γ) Reactions in Fuel-Element Materials

| Material | (n,γ) Reactions per Fission | (n,γ) Reactions per sec per $cm^3$ of Fuel Element per Mw of Reactor Power | |
|---|---|---|---|
| | | Average for Core | Peak for Outer Third-Pass Element |
| | | $\times 10^9$ | $\times 10^9$ |
| $U^{235}$ | 0.2229 | 2.595 | 5.243 |
| $U^{238}$ | 0.3897 | 4.538 | 9.166 |
| Stainless steel | 0.2358 | 2.745 | 5.546 |
| $H_2O$ | 0.06372 | 0.7421 | 1.499 |

Table B.2. Capture Gamma-Ray Spectra

| Group | Energy (Mev) | Energy per Capture (Mev) | | | |
|---|---|---|---|---|---|
| | | Stainless Steel | $U^{238}$ | $U^{235}$ | $H_2O$ |
| 1 | 0.5 | 0.051 | 1.55 | 1.69 | 0 |
| 2 | 1 | 0.275 | 1.28 | 2.00 | 0 |
| 3 | 2 | 0.184 | 1.75 | 1.88 | 2.23 |
| 4 | 4 | 0.915 | 0.20 | 0.71 | 0 |
| 5 | 6 | 1.83 | 0 | 0.13 | 0 |
| 6 | 8 | 4.346 | 0 | 0.02 | 0 |
| 7 | 10 | 0.498 | 0 | 0 | 0 |
| Total | | 8.095 | 4.78 | 6.43 | 2.23 |

Table B.3. Prompt-Fission and Fission-Product Decay Gamma-Ray Spectra

| Group | Energy (Mev) | Energy per Fission (Mev) | |
|---|---|---|---|
| | | Prompt Fission | Fission Product |
| 1 | 0.5 | 1.89 | 1.84 |
| 2 | 1 | 2.24 | 2.31 |
| 3 | 2 | 2.11 | 2.21 |
| 4 | 4 | 0.79 | 0.58 |
| 5 | 6 | 0.15 | 0.06 |
| 6 | 8 | 0.02 | 0.01 |
| 7 | 10 | 0 | 0 |
| Total | | 7.2 | 7.01 |

Table B.4. Gamma-Ray Source Strength

| Group | Energy (Mev) | Gamma-Ray Source Strength per Megawatt (Mev/sec·cm³)[a] | | | | | | | |
|---|---|---|---|---|---|---|---|---|---|
| | | Capture | | Prompt Fission | | Fission Product | | Total | |
| | | Average[b] | Peak[c] | Average[b] | Peak[c] | Average[b] | Peak[c] | Average[b] | Peak[c] |
| | | $\times 10^9$ | $\times 10^9$ | $\times 10^9$ | $\times 10^9$ | $\times 10^9$ | $\times 10^9$ | $\times 10^9$ | $\times 10^9$ |
| 1 | 0.5 | 11.56 | 23.35 | 22.00 | 44.45 | 21.43 | 43.28 | 54.99 | 111.08 |
| 2 | 1 | 11.75 | 23.74 | 26.08 | 52.69 | 26.90 | 54.33 | 64.73 | 130.76 |
| 3 | 2 | 14.98 | 30.26 | 24.57 | 49.63 | 25.73 | 51.98 | 65.28 | 131.87 |
| 4 | 4 | 5.26 | 10.63 | 9.20 | 18.58 | 6.75 | 13.64 | 21.21 | 42.85 |
| 5 | 6 | 5.36 | 10.83 | 1.75 | 3.53 | 0.70 | 1.41 | 7.81 | 15.77 |
| 6 | 8 | 11.98 | 24.21 | 0.23 | 0.47 | 0.12 | 0.24 | 12.34 | 24.92 |
| 7 | 10 | 1.37 | 2.76 | 0 | 0 | 0 | 0 | 1.37 | 2.76 |

[a]Based on volume enclosed by fuel-element containers.

[b]Average for core.

[c]Peak for outer third-pass element.

## Attenuation Coefficients

### Linear Attenuation Coefficients

Linear attenuation coefficients for the homogenized core were obtained by combining the coefficients for the individual constituents according to the formula

$$\mu = \rho \sum_i \left(\frac{\mu}{\rho}\right)_i w_i \quad ,$$

where

$\mu$ = linear attenuation coefficient for the mixture,

$\rho$ = density of mixture,

$\left(\frac{\mu}{\rho}\right)_i$ = mass attenuation coefficient for the ith constituent,

$w_i$ = weight fraction of ith constituent.

The weight fractions and densities for the fuel-element materials are as follows:

| Constituent | $w_i$ (weight fraction) | Density ($g/cm^3$ of mixture) |
|---|---|---|
| Type 304 stainless steel | 0.2090 | 0.9092 |
| $UO_2$ | 0.6864 | 2.9858 |
| $H_2O$ | 0.1046 | 0.4550 |
| Total | 1.0000 | 4.35 |

Attenuation coefficients for individual components and for the homogenized fuel elements are given in Table B.5.

Table B.5. Attenuation Coefficients for Fuel-Element Materials

| Group | Energy (Mev) | $\left(\frac{\mu}{\rho}\right)$ ($cm^2/g$) | | | $\mu$ for Mixture ($cm^{-1}$) |
|---|---|---|---|---|---|
| | | Stainless Steel | $UO_2$ | $H_2O$ | |
| 1 | 0.5 | 0.0840 | 0.1734 | 0.0967 | 0.6381 |
| 2 | 1 | 0.0598 | 0.0762 | 0.0706 | 0.3141 |
| 3 | 2 | 0.0422 | 0.0478 | 0.0493 | 0.2036 |
| 4 | 4 | 0.0330 | 0.0423 | 0.0339 | 0.1718 |
| 5 | 6 | 0.0306 | 0.0445 | 0.0277 | 0.1731 |
| 6 | 8 | 0.0298 | 0.0468 | 0.0242 | 0.1779 |
| 7 | 10 | 0.0300 | 0.0493 | 0.0221 | 0.1844 |

## Energy Absorption Attenuation Coefficients

The energy absorption attenuation coefficients for Zircaloy are shown in Table B.6. Since no tabulation of coefficients was available, the values in Table B.6 were obtained by interpolation in atomic number of data on other elements given by Blizard.[5]

[5]Everitt P. Blizard, "Nuclear Radiation Shielding," Nuclear Engineering Handbook (Harold Etherington, Ed.) McGraw-Hill Book Company, 1958.

Table B.6. Energy Absorption Attenuation Coefficients for Zircaloy

| Group | Energy (Mev) | $\left(\frac{\mu_a}{\rho}\right)$ ($cm^2/g$) | $\mu_a$ ($cm^{-1}$) |
|---|---|---|---|
| 1 | 0.5 | 0.0362 | 0.2340 |
| 2 | 1 | 0.0263 | 0.1699 |
| 3 | 2 | 0.0230 | 0.1486 |
| 4 | 4 | 0.0243 | 0.1570 |
| 5 | 6 | 0.0265 | 0.1712 |
| 6 | 8 | 0.0288 | 0.1860 |
| 7 | 10 | 0.031 | 0.2000 |

## Buildup Factors

As indicated previously, an empirical expression for the buildup factor,

$$B_a(\mu R) = A\ e^{-\alpha_1 \mu R} + (1 - A)\ e^{-\alpha_2 \mu R} \quad ,$$

was used in the heating calculations. The three parameters $\alpha_1$, $\alpha_2$, and A have been tabulated for a few materials.[6] Of course, no tabulation of parameters is available for the peculiar mixture of attenuating materials of interest here. By normalizing the $\mu$ curve for the mixture to 4 Mev and comparing this curve with similar normalizations for other materials, it was found that the attenuation coefficient for the mixture has an energy dependence (at low energies) similar to that of the attenuation coefficient for lead. Thus, the buildup factor for lead should be applicable to the core mixture. Unfortunately, energy absorption buildup factor parameters for lead were not available. Thus, the parameters for iron were used, since iron has the next lowest atomic number for which buildup factor parameters were available. The use of buildup factors for iron results in some overestimate in energy deposition. The buildup factor parameters are given below:

[6]Theodore Rockwell III, Ed., Reactor Shielding Design Manual, TID-7004 (March 1956).

| Group | Energy (Mev) | $\alpha_1$ | $\alpha_2$ | A |
|---|---|---|---|---|
| 1 | 0.5 | −0.0950 | 0.0367 | 15.90 |
| 2 | 1 | −0.0864 | 0.0462 | 11.15 |
| 3 | 2 | −0.0760 | 0.0730 | 6.50 |
| 4 | 4 | −0.0822 | 0.0965 | 3.42 |
| 5 | 6 | −0.0862 | 0.1060 | 2.44 |
| 6 | 8 | −0.0887 | 0.0894 | 1.87 |
| 7 | 10 | −0.0962 | 0.0490 | 1.52 |

## Energy Deposition from Gammas Originating in Fuel Element

Use of the above data on source strength and material properties in Eqs. (7-B) and (8-B) resulted in an energy deposition rate in Zircaloy of $60.66 \times 10^{10}$ Mev/cm$^3$·sec per megawatt of reactor power; this does not include energy deposition from capture gammas which originate in the Zircaloy.

## Energy Deposition from Capture Gammas Originating in Zircaloy

The average binding energy of the last neutron in the product nucleus for naturally occurring zirconium was obtained from

$$\overline{BE} = \sum_i m_i \frac{\sigma_i}{\overline{\sigma}} (BE)_i \quad ,$$

where

$m_i$ = atomic fraction of ith zirconium isotope in natural zirconium,

$\sigma_i$ = thermal neutron microscopic absorption cross section for ith isotope,

$\overline{\sigma}$ = thermal neutron microscopic absorption cross section for natural zirconium,

$(BE)_i$ = neutron binding energy for ith isotope.

The average binding energy was found to be 8.06 Mev.

The ratio of neutron absorption rate density in Zircaloy to the fission rate density in the core was found from four-group diffusion-theory calculations on a typical fuel-element cell.[3] The result is

$$\frac{\text{Absorption rate density in Zircaloy}}{\text{Fission rate density in fuel region}} = 0.1811 \quad .$$

Using the fission rate density and neutron binding energy for zirconium given previously, the energy emission rate density of capture gammas from the Zircaloy is $3.43 \times 10^{10}$ Mev/sec·cm$^3$ per megawatt of reactor power. It was assumed that all gamma rays originating in Zircaloy are deposited in Zircaloy since, even with this assumption, only about 5% of the total gamma-ray energy deposition is from Zircaloy capture gammas.

Total Energy Deposition Rate in Zircaloy

The total gamma-ray energy deposition rates in Zircaloy are given below:

| Reactor Power (Mw) | Energy Deposition in Zircaloy | | |
|---|---|---|---|
| | Mev/sec·cm$^3$ | w/g | Btu/hr·ft$^3$ |
| 1 | $64 \times 10^{10}$ | 0.0159 | $9.91 \times 10^3$ |
| 69 | $4.42 \times 10^{13}$ | 1.097 | $6.84 \times 10^5$ |
| 89.7 | $5.74 \times 10^{13}$ | 1.426 | $8.89 \times 10^5$ |

It should be noted that these figures represent peak values for Zircaloy containers and follower rods located at the boundary separating the second- and third-pass fuel elements.

## Internal Distribution

1-2. T. D. Anderson
3. S. E. Beall
4. M. Bender
5. A. L. Boch
6. R. B. Briggs
7. A. P. Fraas
8. B. L. Greenstreet
9. E. E. Gross
10. P. N. Haubenreich
11. V. O. Haynes
12. S. I. Kaplan
13. O. H. Klepper
14. R. N. Lyon
15. H. G. MacPherson
16. W. D. Manly
17. H. C. McCurdy
18. A. J. Miller
19. S. E. Moore
20. A. M. Perry
21. M. W. Rosenthal
22. G. Samuels
23. H. W. Savage
24. A. W. Savolainen
25. L. D. Schaffer
26. L. R. Shobe
27. M. J. Skinner
28. I. Spiewak
29. J. A. Swartout
30. C. L. Whitmarsh
31. W. C. Thurber
32. M. L. Winton
33. D. B. Trauger
34-35. Central Research Library (CRL)
36-38. Y-12 Document Reference Section (DRS)
39-41. Laboratory Records Department (LRD)
42. Laboratory Records Department (LRD-RC)

## External Distribution

43. R. O. Mehann, States Marine Lines, Incorporated
44-47. J. E. Robb, Division of Reactor Development (Maritime Reactors), AEC, Washington
48-51. R. T. Schomer, The Babcock & Wilcox Company, Atomic Energy Division, Lynchburg, Virginia
52. W. C. Stamm, Ebasco Services, Incorporated, New York, New York
53. Research and Development Division, ORO
54-55. Reactor Division, ORO
56-70. Division of Technical Information Extension (DTIE)